

Chemical Science

Accepted Manuscript

This article can be cited before page numbers have been issued, to do this please use: H. Wang, S. Huan, Z. Chu, Z. Yin and C. Wang, *Chem. Sci.*, 2025, DOI: 10.1039/D5SC04964D.



This is an Accepted Manuscript, which has been through the Royal Society of Chemistry peer review process and has been accepted for publication.

Accepted Manuscripts are published online shortly after acceptance, before technical editing, formatting and proof reading. Using this free service, authors can make their results available to the community, in citable form, before we publish the edited article. We will replace this Accepted Manuscript with the edited and formatted Advance Article as soon as it is available.

You can find more information about Accepted Manuscripts in the [Information for Authors](#).

Please note that technical editing may introduce minor changes to the text and/or graphics, which may alter content. The journal's standard [Terms & Conditions](#) and the [Ethical guidelines](#) still apply. In no event shall the Royal Society of Chemistry be held responsible for any errors or omissions in this Accepted Manuscript or any consequences arising from the use of any information it contains.

Tailoring Flexibility of Nanofluidic Covalent Organic Framework Membranes for Efficient Separation of Gases with Similar Kinetic Diameters

Huijie Wang,^{1†} Shuang Huan,^{1†} Zhenyu Chu,² Zongyou Yin,³ Chen Wang^{1*}

¹State Key Laboratory of Microbial Technology, Jiangsu Collaborative Innovation Center of Biomedical Functional Materials, Jiangsu Key Laboratory of New Power Batteries, School of Chemistry and Materials Science, Nanjing Normal University, Nanjing 210023, China

²State Key Laboratory of Materials-Oriented Chemical Engineering, College of Chemical Engineering, Nanjing Tech University, Nanjing 211816, China;

³Research School of Chemistry, The Australian National University, Canberra, Australian Capital Territory 2601, Australia.

Corresponding E-mail: wangchen@njnu.edu.cn (C. Wang)



Abstract

View Article Online
DOI: 10.1039/D5SC04964D

Conventional nanofluidic membranes often exhibit low selectivities for efficient separation of gases with similar kinetic diameters. Soft nanofluidic membranes overcome this challenge through combination of selective binding sites and tunable pore structures, creating an on-demand separation switch that enables adaptive pore opening for enhanced gas separation. Herein, three different nanofluidic membranes of soft covalent organic framework (named as S-COF1, S-COF2, and S-COF3) with varied flexibility levels was synthesized for similar-sized gases separation using ethane (C_2H_6) and ethylene (C_2H_4) as model gases. The flexibility was precisely tuned by introducing varying numbers of functionalized -OH linkers to form intramolecular [-O-H...N=C] hydrogen bonding. Highly flexible S-COF1 and S-COF2 demonstrated similar pore behavior for C_2H_4 and C_2H_6 , resulting in poor separation efficiency. In contrast, S-COF3, with enhanced rigidity due to the addition of the highest amount of -OH linkers, exhibited distinct pore switching from “close” in C_2H_4 to “open” in C_2H_6 . This led to a C_2H_6/C_2H_4 selectivity of 18.2, which is superior to most of reported membranes. This work establishes a functionalized -OH linker strategy to precisely tune COF flexibility, revealing its critical role in gas separation and advancing the design of dynamic porous membranes.

Keywords: gas separation, nanofluidics, soft covalent organic framework (S-COF), flexibility regulation, ethane/ethylene separation



Introduction

Ethylene is the most crucial feedstock in petrochemical production systems, extensively used to produce polypropylene, plastic materials, and diverse industrial chemical commodities.¹⁻⁵ However, the presence of even a small amount of ethane in ethylene production can severely disrupt further ethylene polymerization, highlighting the urgent need to develop alternative technologies for effective C₂H₆ separation to achieve pure-grade C₂H₄.⁶⁻⁹ Nanofluidic separation membranes provide a more cost-effective and energy-efficient gas purification method.^{10,11} The ideal gas separation membranes often use the size exclusion effect, but still remains challenging for efficient separation of gases with similar sizes like ethane and ethylene owing to the intricate task of precisely controlling pore size.² Recently, our group developed carboxylic acid-based HOF membranes with adjustable pore sizes (6.2-24 Å) that achieved exceptional H₂/CO₂ separation (up to 164) through synergistic size exclusion and electrostatic interactions.¹² However, even precisely tuned pore apertures show limited efficacy for C₂ hydrocarbon separations due to their minimal size differentiation. To address this challenge, researchers drew inspiration from natural membrane systems and found that stimuli such as light and pressure can elicit the transition between “open” and “closed” conformations, enabling the regulation of ion transport.¹³⁻¹⁵ Similarly, gas separation membranes can leverage this property by combining guest-specific adsorption with a flexible internal structure design, creating unique functionality.¹⁴ This strategy provides an “on-off” separation method that eliminates the need to precisely control the aperture size and instead relies on highly sensitive object-dependent threshold pressures.¹⁶ However, porous materials with this property are limited, and most of them are focused on flexible metal-organic framework (MOF) and hydrogen-bonded organic framework (HOF) that face stability issues during multiple cycles.¹⁷⁻¹⁹ Therefore, the development of new robust porous membrane materials with gate-opening functions is critical.

Covalent organic framework (COF) are crystalline porous materials constructed from organic precursors via covalent bonds and have recently attracted extensive

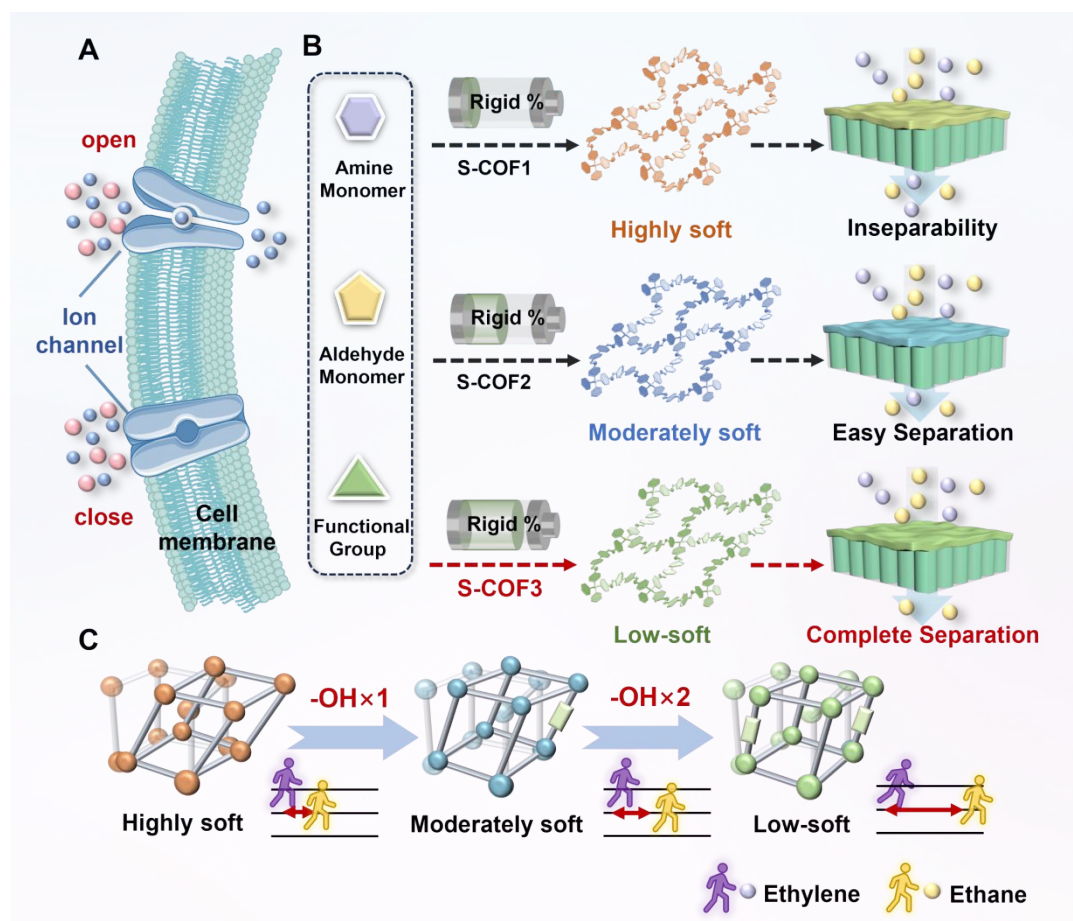


research attention for precise gas separation owing to their periodic architectures and tunable pore environments.²⁰ Compared with MOF based on coordination bonds and HOF relying on hydrogen bonds, the superior covalent bond strength of COF ensures their enhanced framework stability.^{19,21-24} This stability enables COF to maintain the integrity of its pore structure during host-guest interactions and under operational pressure. Consequently, COF are considered more suitable for gas separation as flexible porous materials. Current research primarily focuses on synthesizing flexible COF,^{25,26} neglecting the precise control of flexibility to enhance separation performance.^{27,28} Meanwhile, there is a lack of effective strategies for tuning framework flexibility, and the impact of flexibility on membrane performance remains largely unexplored.^{17,18} Notably, numerous flexible porous materials have been reported, which are able to recognize highly polar molecules, such as C₂H₂ and C₂H₄.²⁹ However, for feed gases containing less C₂H₆ and more C₂H₄, C₂H₆-selective membranes used for purifying C₂H₄ products can achieve separation with higher efficiency. Despite this, achieving the preferential recognition separation of inert C₂H₆ from C₂H₄ mixtures through a flexible adsorption mechanism remains a challenge.

Herein, three soft covalent organic framework (S-COF) membranes were in-situ grown on anodized aluminum oxide (AAO) for gas separation (Scheme 1). By incorporating functionalized 4,4'-biphenyl-dicarboxaldehyde derivatives with different numbers of -OH groups, three S-COF nanofluidic membranes (termed highly soft S-COF1, moderately soft S-COF2, and low-soft S-COF3 membrane) with varying degrees of flexibility have been utilized for the challenging C₂H₆/C₂H₄ separation. Specifically, the incorporation of -OH groups adjacent to the [-C=N] centers in S-COF2 and S-COF3 facilitated the formation of intramolecular [-O-H...N=C] hydrogen bonds, which effectively reduced the flexibility of the membrane and optimized its separation performance.³⁰ Moreover, the pore environment of the flexible S-COF membrane is rich in low-polarity aromatic rings and uncoordinated N and O atoms, which enable strong interaction with ethane molecules, thus giving the nanofluidic membrane excellent affinity for ethane.³¹⁻³⁵ Therefore, the flexible S-COF3 membrane transitioned from closed-pore state to opened-pore state structures as the guest molecules changed



from C_2H_4 to C_2H_6 , achieving a C_2H_6/C_2H_4 selectivity of 18.2, significantly higher than that of the S-COF1 membrane (4.7) and the S-COF2 membrane (8.5). This is because the flexibility of the S-COF3 membrane is regulated by hydrogen bond interactions, resulting in the largest gated-pressure gap between ethane and ethylene. In contrast, S-COF1 and S-COF2, with higher flexibility, show similar pore behavior for C_2H_4 and C_2H_6 , leading to poor separation efficiency. To the best of our knowledge, this is the first report on the preferential permeation of ethane over ethylene through flexible S-COF membrane. This work represents the first instance of gradually tuning flexibility of nanofluidic membranes for gases separation, offering a novel approach to advancing industrial gas purification technology.



Scheme 1. (A) Inspired by the “open” and “closed” conformational transitions in natural membrane systems. (B) Three S-COF membranes (S-COF1, S-COF2, and S-COF3) with different amount of functionalized -OH linkers were synthesized for gas separation. (C) Schematic illustration of the gas separation principle by flexible S-COF membranes.

Results and Discussion



2.1 Synthesis and characterization of S-COF

View Article Online
DOI: 10.1039/D5SC04964D

The design of highly soft COF (S-COF1), moderately soft COF (S-COF2), and low-soft COF (S-COF3) enabled stepwise regulation of COF membrane flexibility through functional group modulation strategies. To optimize the functionalized S-COF, the flexibility of these three S-COF was precisely tuned by introducing varying numbers of functionalized -OH linkers (Figure 1A). The incorporation of -OH functionalities adjacent to the [-C=N] centers in S-COF2 and S-COF3 led to the formation of intramolecular [-O-H...N=C] hydrogen bonding and reduced the degree of flexibility.³⁶⁻³⁸ The S-COF1 were synthesized according to the literature reported previously, while S-COF2 and S-COF3 were synthesized using 4,4'-biphenyl-dicarboxaldehyde derivatives with single and dual hydroxyl groups as building blocks, respectively.¹⁹ The crystalline structures were proved by powder X-ray diffraction (PXRD, Figures 1B-1D, Figure S1) and Fourier transform infrared (FT-IR) spectroscopy (Figures 1E-1G). The XRD patterns matched well with those of the simulated data, demonstrating the successful formation of the expected crystal structure. For the FT-IR results, the disappearance of the representative stretching vibration of C=O (1680 cm^{-1}) and N-H stretching vibration of amines ($3100\text{-}3400\text{ cm}^{-1}$) in the S-COF alongside the generation of C=N stretching vibration peak around 1620 cm^{-1} revealed the successful formation of imine-based S-COF, which were consistent with the previous reports.³⁹ In addition, thermogravimetric analysis (TGA) shows that the three S-COF are thermally stable up to $300\text{ }^{\circ}\text{C}$ (Figure S2). This ensures the vacuum degassing of the S-COF at high temperatures to obtain the guest free S-COF membrane structure and stability under high temperature separation conditions.³¹ The characterizations above confirm the successful preparation of a series of flexible S-COF with similar framework structures but different degrees of flexibility, providing the necessary conditions for subsequent gas separation.



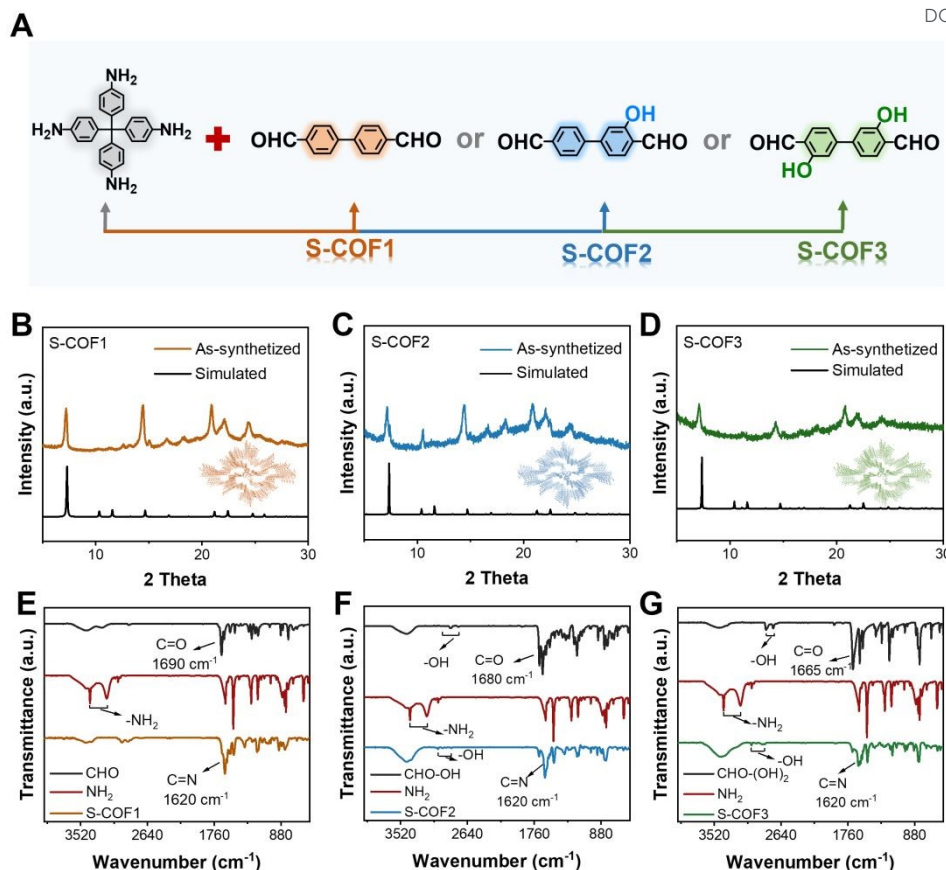


Figure 1. Synthesis and characterization of S-COFs. (A) Scheme for the preparation of S-COF1, S-COF2 and S-COF3. (B-D) Powder X-ray diffraction of (B) S-COF1, (C) S-COF2, and (D) S-COF3. (E-G) FT-IR spectra of (E) S-COF1, (F) S-COF2, and (G) S-COF3.

The preparation of continuous, defect-free membrane is crucial for achieving highly selective gas separations.²¹ Figure 2A illustrates the fabrication process of the S-COF membrane. First, the anodic aluminum oxide (AAO) was fabricated using the anodization oxidation technique (Figure S3).^{40,41} As shown in Figures 2B and 2C, the fabricated AAO substrate exhibited regular nanochannels with a diameter of around 50 nm. After immersion in (3-aminopropyl) triethoxysilane (APTES) solution for 12 hours, the AAO surface achieved successful amine functionalization. XPS characterization confirmed this modification through the emergence of a distinct (-Si-O-) signal at 101.5 eV (Figure S4), absent in pristine AAO substrates.³⁹ The amino-functionalized AAO substrate was then reacted with the aldehyde groups in 4,4'-biphenyldicarboxaldehyde to a functional layer via amide bond formation, as confirmed by Attenuated Total Reflectance (ATR) - Fourier Transform Infrared (FTIR) spectroscopy (Figure S5).



Subsequently, the complete S-COF membrane was formed on the AAO surface by adding tetrakis(4-aminophenyl)methane and heating at 65 °C for seven days. ATR-FTIR spectroscopy in Figure S6 revealed characteristic peaks of C=N stretching vibrations, verifying the successful formation of imine bonds in the S-COF membrane. The zeta potential measurements reflect the surface charge of the material. As shown in Figure S7, the introduction of hydroxyl groups reduced the positive charge of the S-COF, attributed to the negative charge of hydroxyl groups. Additionally, Figure S8 showed that the addition of hydroxyl groups reduces the water contact angle, indicating enhanced hydrophilicity. These characterizations provide clear evidence for the successful synthesis and functionalization of three S-COF membranes.^{39,42}

Scanning electron microscopy (SEM) was used to characterize the morphology of membrane. Figures 2D-2F demonstrated the successful fabrication of the S-COF membrane, with S-COF covering the top surface of AAO. Additionally, the cross-section image of S-COF1 membrane demonstrated successful preparation of S-COF layers \approx 200 nm thick, which was densely attached to the top of AAO layer (Figure 2D). With the same procedure, S-COF2 and S-COF3 membranes were readily synthesized (Figures 2E-2F). Notably, the thickness of the prepared S-COF layer can be facilely and precisely controlled via the duration of growth. During the first four days, monomers reacted at the solid-liquid interface of the AAO surface, but the initial material deposition did not fully cover the substrate (Figures S9-S12). When the growth time was extended to 7 days, a continuous S-COF membrane without obvious defects formed, with thicknesses ranging from 100 nm to 280 nm (Figures S13-S18). Therefore, considering factors such as membrane thickness and gas separation performance, S-COF membrane prepared for 6 days, with a thickness of approximately 200 nm, was selected for subsequent characterization and tests. More visually intuitive, the digital photos of S-COF membrane showed its structural integrity (Figure S19). Energy dispersive X-ray spectroscopy (EDS) confirmed the presence of functional groups, and Figures 2G-2I showed the uniform distribution of C, N, and O elements in the S-COF membrane structure (note that S-COF1 lacked O), indicating successful formation of the S-COF layer on the AAO surface. Atomic-force-microscopy (AFM) analysis



further confirmed the smooth and homogeneous surface morphology of the S-COF membrane (Figure S20). To evaluate the mechanical robustness and interfacial adhesion, the S-COF membrane was subjected to ultrasonication. Post-sonication characterization via SEM confirmed that the membrane layer remained completely intact without any cracks, delamination, or detachment, indicating strong interfacial interaction and robust mechanical integrity (Figures S21-S22). Furthermore, FT-IR analysis confirmed the preservation of the C=N covalent bonding within the S-COF structure across the coated area after this treatment, providing direct evidence of the chemical and mechanical stability at the membrane-substrate interface (Figure S23). In summary, three S-COF membranes with different degrees of flexibility were successfully fabricated.

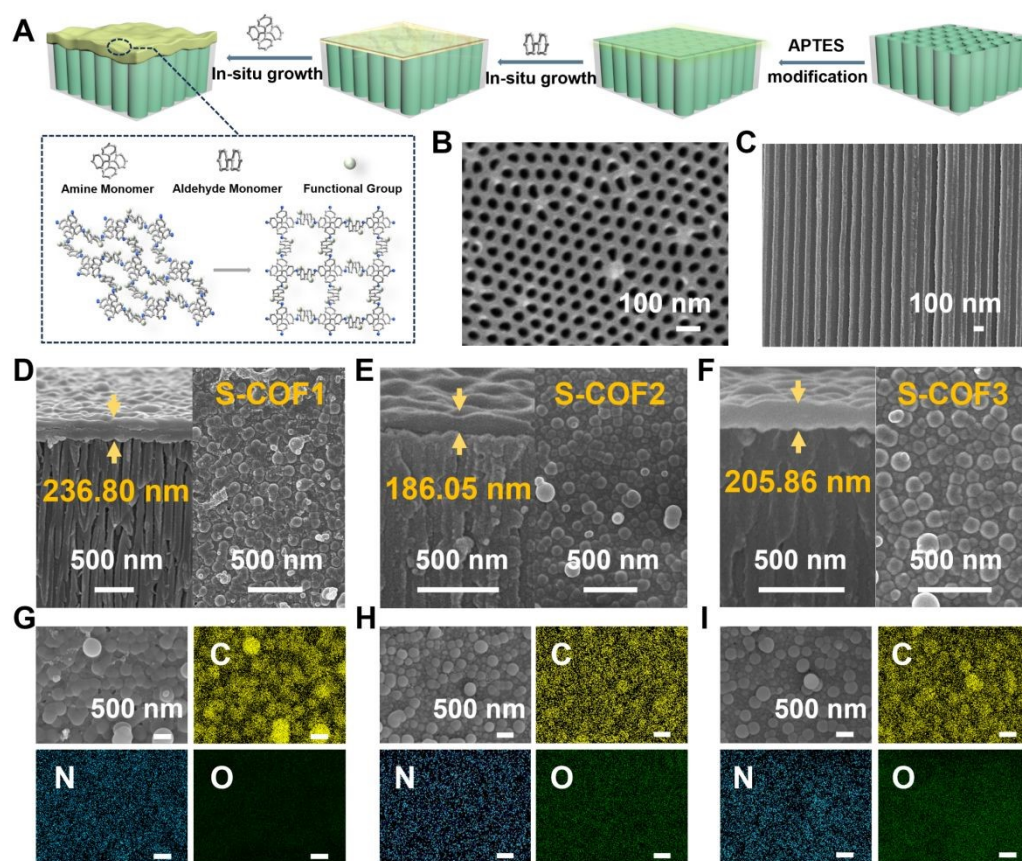


Figure 2. Fabrication and characterization of flexible S-COF membranes with gate-opening mechanism. (A) Schematic illustration of the fabrication process of S-COF membrane. (B-C) SEM images for (B) the top and (C) cross-sectional view of AAO. (D-F) SEM images of the (D) S-COF1, (E) S-COF2, (F) S-COF3 membrane (left: cross-section; right: top). (G-I) SEM image of the (G) S-COF1, (H) S-COF2, (I) S-COF3 corresponding energy-dispersive X-ray (EDX) elemental mappings of C, N and O.



2.2 Gas adsorption of S-COF

View Article Online
DOI: 10.1039/D5SC04964D

Flexible S-COF membranes provide a switching method strategy to achieve molecular sieving without the need for precise control of pore size, but instead relying on highly sensitive guest dependent threshold pressure (Figure 3A).^{16,43} To evaluate the porous structure of S-COF, the N₂ sorption isotherm was performed at 77 K (Figures S24-S26). Notably, the isotherms of S-COF showed typical closed-pore to opened-pore transition. In the case of S-COF-1, negligible N₂ uptake occurred below 0.5 bar while the uptake reached 687 cm³ g⁻¹ at 1 bar. The flexible nature of the material enables its pores to dynamically adjust during the adsorption process, expanding to accommodate more gas molecules. Similar dynamic adsorption behaviors were also observed in S-COF2 and S-COF3 (Figures S25-S26). S-COF2 exhibited negligible N₂ adsorption below 0.55 bar (Figure S25), but underwent a pressure-activated adsorption transition at 0.55 bar. The N₂ uptake subsequently increased gradually with pressure, attaining an adsorption capacity of 517 cm³ g⁻¹ at 1 bar (Figure S25). Similarly, S-COF3 remained in a closed-pore state toward N₂ adsorption at 77 K when pressure was below 0.65 bar. Nonetheless, phase transformation to the open pore structure occurred at 0.65 bar (Figure S26). The N₂ adsorption capacity at 77 K was determined to be 395 cm³ g⁻¹ at 1 bar. In summary, the gradual increase in pore-opening pressure from S-COF1 to S-COF3 can be attributed to the progressive incorporation of -OH groups. The introduction of more -OH linkers in S-COF3 enhances the rigidity of the framework, resulting in higher pressure thresholds required to activate the porous structure. This trend highlights the significant role of -OH linkers in modulating the flexibility and pore accessibility of S-COF membranes. To better characterize the micropores, adsorption isotherms of S-COF were tested using the smaller gas molecule CO₂ as the probe (Figures 3B-3D and Figure S27). Adsorption at 195 K reached P/P₀ = 1, enabling more accurate detection of micropores. BET specific surface area analysis indicates that the specific surface areas of S-COF1, S-COF2, and S-COF3 are 322 m² g⁻¹, 218 m² g⁻¹, and 155 m² g⁻¹, respectively.

Subsequently, the single-component isotherms of flexible S-COF for C₂H₆ and



C_2H_4 adsorption were measured, as shown in Figures 3E-3G. Before the adsorption measurements, a vacuum was pumped under a dynamic vacuum to obtain the state of S-COF pore closure.⁴⁴ S-COF1 exhibited a closed-pore state structure for C_2H_6 adsorption under low pressures (<0.39 bar), which transitioned to an open-gated state at a critical pressure of 0.39 bar at 298 K (Figure 3E). This structural transition triggered an abrupt surge in C_2H_6 uptake with increasing pressure, ultimately reaching adsorption saturation at approximately 0.8 bar. Similarly, the gate-opening pressures for C_2H_6 were 0.42 bar in S-COF2 and 0.75 bar in S-COF3, highlighting a substantial increase compared to S-COF1 (Figures 3F-3G). These findings indicate that the threshold pressures can be adjusted by varying the number of -OH functional groups to gradually controlling the number of intramolecular [-O-H \cdots N=C] hydrogen bonding. Superior C_2H_6 affinity of S-COF originates from a pore environment enriched by hydroxyl groups whose oxygen centers act as strong hydrogen bond acceptors for ethane, enhancing C-H \cdots O interaction with ethane over ethylene and enabling selective recognition.³³⁻³⁵ These results demonstrate that the gating pressure can be effectively controlled by varying the number of -OH functional groups introduced, providing conditions for ethane and ethylene membrane separation.



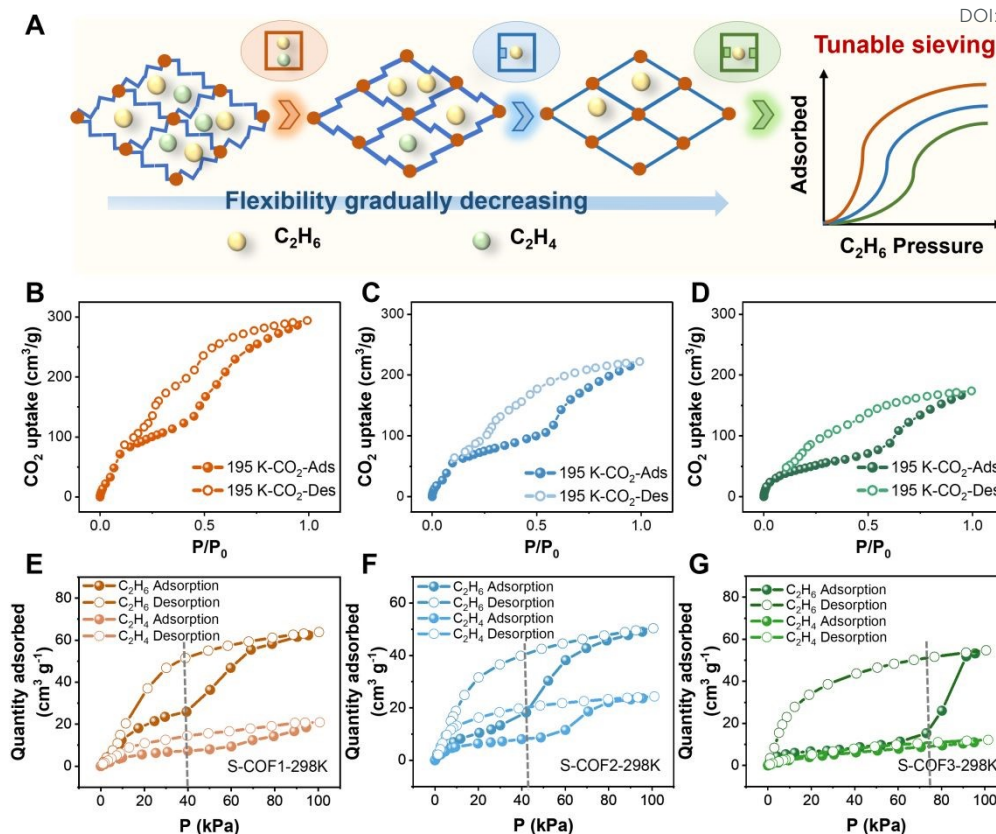


Figure 3. Investigation of flexible S-COF gas adsorption and separation with gate-opening mechanism. (A) Schematic diagram of different degrees of flexibility and the gas adsorption separation in flexible S-COF. (B-D) Adsorption isotherm of CO_2 (195 K) for (B) S-COF1, (C) S-COF2 and (D) S-COF3. (E-G) C_2H_6 and C_2H_4 adsorption isotherms of (E) S-COF1, (F) S-COF2 and (G) S-COF3 at 298 K.

2.3 Gas separation performance and mechanism

The selective adsorption properties of flexible S-COF and the operational advantages of membrane technology have driven us to further investigate C_2H_6/C_2H_4 separation in flexible S-COF-based membranes. Before the gas permeation test, the as-prepared S-COF membranes were activated in the vacuum oven at 100 °C for 12 h. The C_2H_6/C_2H_4 separation performance of flexible S-COF membrane was evaluated through measurements of both single (C_2H_6 or C_2H_4) and binary gas permeation at 25 °C using our homemade Wicke-Kallenbach setup (Figure 4A, Figure S28).⁴⁵ The bare AAO disk demonstrated extremely high gas permeance for all gases under study, and its low gas separation selectivity had been calculated, thus eliminating the influence of



AAO support on gas separation (Figure S29). First, single-component tests were conducted to determine how the thickness of the flexible S-COF membrane influences permeance and selectivity, with the goal of achieving an optimal balance between these two parameters. As the growth time of the membrane was increased from 3 to 7 days, the permeability of C_2H_6 and C_2H_4 decreased, while the C_2H_6/C_2H_4 selectivity initially increased and then remained constant. (Figures S30-S32). Therefore, considering the tradeoff between permeability and selectivity, flexible S-COF membranes prepared for 6 days were selected for subsequent tests. Single-component gas separation experiment was carried out to evaluate the ideal separation performance of S-COF membrane. The permeation of gas molecules with different kinetic diameters (H_2 , CO_2 , N_2 , C_2H_4 , and C_2H_6) through flexible S-COF membranes was evaluated (Figure 4B), demonstrating that C_2H_6 permeation rates were higher than those of C_2H_4 due to effective recognition. Moreover, the flexible S-COF3 membrane exhibited H_2/CO_2 , CO_2/N_2 , H_2/N_2 , C_2H_6/C_2H_4 selectivity all significantly exceeded the corresponding Knudsen selectivity (Figure 4C, Figure S33). This confirms the presence of few grain boundary defects in the membrane. Notably, S-COF3 membranes with specific recognition of C_2H_6 presented high C_2H_6/C_2H_4 selectivity compared to S-COF1 and S-COF2 membranes due to the best gating against ethylene and ethane.

The influence of sweep gas flow rate on membrane performance was systematically evaluated to ensure measurement accuracy (Figure S34). A flow rate of 25 mL min^{-1} was identified as optimal, effectively eliminating concentration polarization on the permeate side while avoiding excessive dilution that would compromise detection sensitivity. All permeation tests were therefore conducted at this standardized flow rate to ensure reliable measurement of intrinsic membrane properties. Subsequently, binary gas permeation tests further demonstrated that the S-COF3 membrane also has advantages in the separation of C_2H_6 and C_2H_4 gas mixture (Figure 4D, Figures S35-S36). The pressure responsive gas separation performance of flexible S-COF was further evaluated using mixed gas feed with various C_2H_6 partial pressures. The flexible S-COF1 membrane showed a low dependence of selectivity on C_2H_6 partial pressure. In contrast, flexible S-COF2 membrane underwent a sudden jump of



C_2H_6/C_2H_4 selectivity when the C_2H_6 partial pressure was increased above 0.4 bar and an abrupt jump at 0.6 bar for flexible S-COF3 membrane (Figure 4E). By controlling pressure-responsive phase transition of the S-COF3, C_2H_6 -induced gate opening behaviors are observed in the resultant membranes, which are accompanied with the sharp increase of C_2H_6 permeance (from 30 to 90 gas permeation units) as well as C_2H_6/C_2H_4 selectivity (from 2 to 18.2). S-COF1 and S-COF2 membrane exhibit low selectivity due to their high flexibility and small gated pressure differences between ethane and ethylene. In contrast, the regulated S-COF3 membrane enhances framework rigidity through intramolecular $[-O-H\cdots N=C]$ interactions. More importantly, the hydroxyl-functionalized pores preferentially strengthen $[C-H\cdots O]$ interactions with ethane over ethylene, as the oxygen atom in the hydroxyl group acts as a strong hydrogen bond acceptor toward ethane molecules, thereby facilitating selective ethane recognition.^{33-35,46} To conclusively determine the gate-opening behavior, gas permeation measurements for C_2H_6 was conducted using helium as a balance gas. The results unequivocally demonstrate that the S-COF3 membrane exhibits a distinct gate-opening transition at approximately 0.6-0.7 bar for C_2H_6 (Figure S37). This confirms that the enhanced permeance is due to specific ethane-induced structural transitions rather than non-selective effects. As a result, different degrees of S-COF membrane flexibility led to different dynamic behaviors, whereas S-COF3 membrane increases selectivity due to the most suitable gated pressure between ethane and ethylene, respectively. In addition, schematic diagram conducted to elucidate the flexible behaviors and separation mechanisms (Figure 4F). During the ethane/ethylene separation process, the membrane preferentially adsorbs ethane. As more ethane molecules are adsorbed, the host-guest interaction energy increases. When this energy exceeds the deformation energy of the host framework, the gate opens to ethane molecules (corresponding to the jump pressure in the gas adsorption isotherm), rendering the membrane permeable to ethane and allowing it to pass through smoothly.^{19,47} The adjusted S-COF3 membrane, with its broad range of ethane and ethylene gated pressures, effectively addresses the complex separation requirements of such mixtures.

View Article Online
DOI: 10.1039/D5SC04964D



To clarify the diffusion pathway within the S-COF membranes, permeation data were split into sorption and diffusion terms, and the results are summarized in Table S1. As expected, the S-COF3 membrane shows higher diffusion and absorption coefficients for C_2H_6 than for C_2H_4 . Moreover, it exhibits the highest diffusion selectivity and solubility selectivity for C_2H_6/C_2H_4 , at 4.87 and 3.83 respectively. This indicates that the membrane's superior separation performance for C_2H_6 and C_2H_4 can be attributed to its preferential diffusion and adsorption of C_2H_6 over C_2H_4 . Subsequently, to investigate differences in mass-transfer kinetics of adsorbed species on S-COF3, time-dependent sorption rate measurements for C_2H_6 and C_2H_4 were conducted at 298 K and 1 bar. As shown in Figure S38, equilibrium sorption on S-COF3 was attained within 31 min for C_2H_6 , markedly faster than the approximately 60 min required for C_2H_4 . Consequently, the diffusion time constant (D/r^2) on S-COF3 was determined to be $9.81 \times 10^{-4} \text{ s}^{-1}$ for C_2H_6 and $4.65 \times 10^{-4} \text{ s}^{-1}$ for C_2H_4 . These results demonstrate that S-COF3 exhibits rapid sorption kinetics and excellent mass-transfer performance, making it a promising candidate for efficient C_2H_6/C_2H_4 separation.

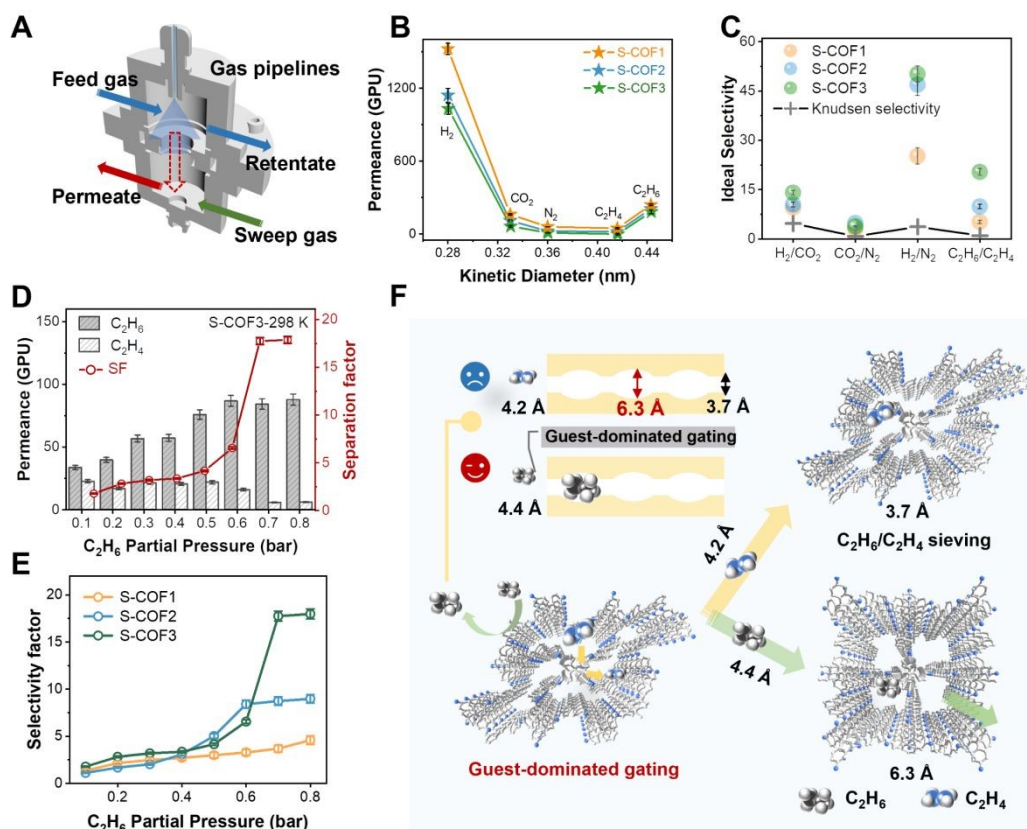


Figure 4. Single-gas and binary-gas C_2H_6/C_2H_4 separation performance of S-COF membranes with varying degrees of flexibility. (A) Home-made gas-permeance module and schematic illustrating



gas transport through the S-COF membrane. (B) H_2 , CO_2 , N_2 , C_2H_4 and C_2H_6 single-component gas permeance of S-COF membranes with different degrees of flexibility at 1 bar. (C) The ideal selectivity of H_2/CO_2 , CO_2/N_2 , H_2/N_2 and C_2H_6/C_2H_4 gas pairs of S-COF membranes with different degrees of flexibility. (D) Effect of C_2H_6/C_2H_4 molar ratios on the separation performance of S-COF3 membrane at 298 K. (E) The separation performances of binary C_2H_6/C_2H_4 gases for the membrane of S-COF1, S-COF2 and S-COF3. (F) Schematic diagram of the guest-dominated gated adsorption separation mechanism.

Membrane stability is regarded as one of the decisive criteria for industrial application.⁴⁸ Extensive testing of performance stability was carried out to explore the practicality of the S-COF membrane (Figure 5A). After continuous operation for 60 h, both C_2H_6 permeance and C_2H_6/C_2H_4 selectivity remained unchanged, which was indicative of excellent operation stability (Figure 5B, Figures S39-S40). PXRD analysis of the S-COF3 membrane after cyclic testing confirmed the intact structure of S-COF (Figure 5C), while FT-IR spectra further demonstrated its structural stability (Figure 5D). SEM images after performance testing (Figure S41-S42) revealed that the membrane remained intact and stable. Significantly, the operational stability of the S-COF3 membrane was further evaluated under demanding conditions to assess its practical relevance. We employed the S-COF3 membrane for C_2H_6/C_2H_4 separation under conditions of 100 °C and 1 bar pressure over 30 hours. During the entire test period, gas permeability increased moderately with rising temperature, while selectivity exhibited only slight fluctuations (Figure S43). In addition, the S-COF3 membrane remained intact in morphology and crystallinity after seven days in water at 25 °C and exhibited only minor, fully reversible loss of C_2H_6/C_2H_4 selectivity under high humidity, confirming excellent hydrolytic stability (Figures S44-S48). The image presented in Figure S19 indicates that the S-COF3 membrane is suitable for scalable fabrication, with the ultimate dimensions principally constrained by the size of the substrate employed. The prepared S-COF3 membrane has an area of approximately 6 cm² and demonstrates consistent performance stability, as shown in Figure S49. As shown in Figure 5E, the SF of C_2H_6/C_2H_4 reached 18.2, which was superior to the majority of other membranes (Figure 5E and Tables S2-S3). Gas permeation data are reported as thickness-normalized permeability (Barrer), determined from independently measured



membrane thicknesses. To facilitate direct and industrially relevant comparison with literature, separation performance was assessed using an equimolar (50/50) C_2H_4/C_2H_6 feed mixture.⁴⁹ The resulting data, along with a categorized comparison of ethane-selective and ethylene-selective membranes from literature, are summarized in Table S3. Thus, S-COF3 membrane was used as a potential separation membrane with high stability and reusability.

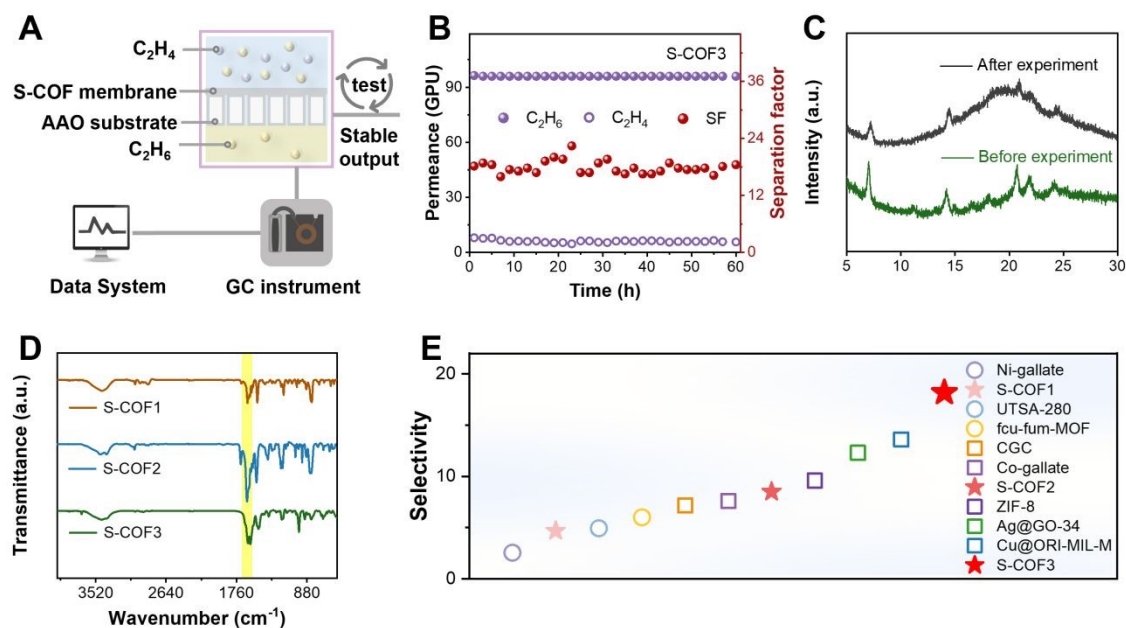


Figure 5. The stability of flexible S-COF membrane under varying operational conditions. (A) Stability diagram of cycle experiment. (B) Long-term separation stability of S-COF3 membrane. (C) PXRD patterns of S-COF3 membrane before and after experiment. (D) FT-IR spectra of S-COF3 membrane after experiment. (E) The performance comparison of the separation between the prepared membranes in this work with other reported membranes in the literature.

Conclusion

In summary, a stepwise structural transformation strategy has been proposed to gradually tune flexibility of nanofluidic S-COF membranes. Three S-COF membranes with similar framework structure but different flexibility were fabricated through introducing varied amounts of functional -OH groups. Among the three types of flexible S-COF membranes, S-COF3 membrane achieved the highest C_2H_6/C_2H_4 selectivity (18.2) due to its optimal flexibility, specific binding site and wide range of ethylene ethane gated-pressures, significantly exceeding the 4.7 of S-COF1 membrane and the



8.5 of S-COF2 membrane. This separation capability significantly outperforms the majority of reported membrane-based separation systems. In addition, the obtained membranes have excellent long-term stability, and these results reveal the great application potential of flexible membrane materials based on S-COF in achieving important gas separation. This expands the application of soft S-COF in membrane separation and proposes regulating gated-pressure for the development of flexible membranes that specifically identify gases, encouraging further research into the design of novel soft COF membranes for industrial gas separation applications.

Experimental Section

Materials and Reagents: Tetrakis(4-aminophenyl) methane (99.99%), 4,4'-Biphenyldicarboxaldehyde (99.99%), 5-(4-ForMylphenyl)-2-forMylphenol (99.99%), 4,4'-Biphenyldicarboxaldehyde, 3,3'-dihydroxy- was purchased from Bide Pharmatech Co., Ltd. Analytical-reagent grade potassium hydroxide (KOH), (3-Aminopropyl) triethoxysilane (APTES) was bought from Sigma Aldrich (Shanghai, China). The aluminum foil has a thickness of 0.1 mm and a purity of 99.999 %, from the General Research Institute of Nonferrous Metals (Beijing, China).

Instrumentation: The morphology of the top and cross-section of membrane was characterized using a scanning electron microscopy (SEM, S-4800, Hitachi, Japan). X-ray diffraction (XRD, SmartLab, Japan) pattern was carried out in the 2θ range of 5° to 30° at room temperature. The water static contact angle was measured by a contact angle system (Kruss-DSA25B, Germany). XPS spectra was performed using Kratos AXIS SUPRA (Shimadzu, Japan).

Synthesis of AAO: The AAO membrane was fabricated via a two-step anodization process. Initially, the aluminum foil was ultrasonically cleaned in acetone and 1 M KOH for 10 min each, followed by rinsing with water. The first anodization was performed at 50 V for 0.5 hours using 0.3 M oxalic acid as the electrolyte. To remove the irregular oxide layer, the anodized foil was treated with a mixture of 6 wt% H_3PO_4 and 1.8 wt% H_2CrO_4 at 60°C for 40 min. The second anodization was then conducted



for 4 hours under the same conditions as the first. The aluminum substrate was etched away using a saturated SnCl_2 solution. The barrier layer was removed by treating the AAO membrane with 1.8 wt% H_3PO_4 for 40 minutes. The membrane was subsequently immersed in boiling 30% H_2O_2 for 30 minutes to introduce -OH groups on the channel surface. Finally, the AAO membrane was soaked in water overnight and dried.

Fabrication of S-COF membrane: The AAO surface was modified by immersion in a (3-aminopropyl) triethoxysilane (APTES) solution for 12 hours. The amine-functionalized AAO was then placed at the bottom of a reaction bottle. S-COF membranes were synthesized on the AAO support via an in-situ growth method. Specifically, 4,4'-biphenyl-dicarboxaldehyde (20 mg) was dissolved in 1,4-dioxane (0.5 mL), followed by the addition of acetic acid (95 μL) in deionized water (0.46 mL). Subsequently, tetrakis(4-aminophenyl) methane (20 mg, 0.053 mmol) in 1,4-dioxane (1.0 mL) was added to the mixture. The mixture was heated at 65°C for seven days in a vial under ambient conditions. The resulting S-COF1 membrane was washed with tetrahydrofuran and dried under vacuum. Similarly, S-COF2 and S-COF3 membranes were prepared using analogs of 4,4'-biphenyl-dicarboxaldehyde: 5-(4-formylphenyl)-2-formylphenol (21.5 mg) and 3,3'-dihydroxy-4,4'-biphenyldicarboxaldehyde (23 mg), respectively.

Gas permeation tests: The gas permeation performance of the membranes was assessed using the Wicke-Kallenbach method. To exclude areas that did not undergo the IP process (due to sealing issues), the membranes were sandwiched between two pieces of aluminum foil tape, with the margins further sealed using a sealant. For the mixed gas separation performance test, the flow rates of equimolar mixed feedstocks were controlled by mass flow controllers, maintaining a total volumetric flow rate of 100 mL/min (50 mL/min for each gas). Argon (25 mL/min) was used as the sweep gas on the permeate side to transport the permeate gas to an on-line gas chromatograph (Panna). The mixed gas separation test was conducted at increasing temperatures with a heating rate of 1 °C/min. For single gas permeation tests, each gas had a flow rate of 100



mL/min, while the sweep gas flow rate was kept at 25 mL/min. The gas permeance of the membrane was calculated as equation:

$$P_i = \frac{N_i}{A\Delta P_i} \quad (1)$$

where P_i represents the permeance of component i ($\text{mol}\cdot\text{m}^{-2}\cdot\text{s}^{-1}\cdot\text{Pa}^{-1}$), N_i is the permeate rate of component i ($\text{mol}\cdot\text{s}^{-1}$), A is the effective membrane area (m^2), and ΔP_i is the transmembrane pressure difference for component i (Pa).

The mixed gas separation factor (SF, α_{ij}) was calculated by the following equation:

$$\alpha_{i,j} = \frac{y_i/y_j}{x_i/x_j} \quad (2)$$

where y_i , y_j , x_i , and x_j are the molar ratios of component i and component j in the permeate and feed side, respectively.

Calculation of adsorption coefficient and diffusion coefficient of different gases: The permeation of gases through membranes is governed by a coupled sorption–diffusion mechanism. Thus, the gas permeability coefficient, P , is expressed as the product of the diffusivity coefficient D and the solubility coefficient S :

$$P=D\times S \quad (3)$$

The value of P is obtained by multiplying the gas permeance by the effective thickness of the MOF membrane, and is reported in Barrer. The solubility coefficient S can be derived from the adsorption isotherm measured at 298 K and 1 bar, in conjunction with the crystalline density of S-COF, using the relation $S=A\times\rho/P_r$, where A represents the adsorption capacity (cm^3/g), ρ denotes the crystalline density of S-COF3, and P_r is the adsorption pressure in cmHg.

Data Availability

The data that support the findings of this study are available within the article and Supplementary Information files, and are also available from the authors upon request.



Author contributions

Chen Wang, Huijie Wang, and Shuang Huan conceived and supervised the project. Huijie Wang, and Shuang Huan performed experiments. All the authors discussed the experimental data. Chen Wang revised the manuscript.

Conflict of Interest

H.W. and S.H. contributed equally to this work. The authors declare no conflict of interest.

Acknowledgements

This work was supported by the National Key Research and Development Program of China (2025YFC3409400), the National Natural Science Foundation of China (22274076), and the Primary Research and Development of Jiangsu Province (BE2022793).

Notes and references

1. T. Xu, P. Zhang, F. Cui, J. Li, L. Kan, B. Tang, X. Zou, Y. Liu and G. Zhu, Fine-Tuned Ultra-Microporous Metal–Organic Framework in Mixed-Matrix Membrane: Pore-Tailoring Optimization for C₂H₂/C₂H₄ Separation, *Adv. Mater.*, 2023, **35**, 2204553.
2. L. Li, R.-B. Lin, R. Krishna, H. Li, S. Xiang, H. Wu, J. Li, W. Zhou and B. Chen, Ethane/ethylene separation in a metal-organic framework with iron-peroxo sites, *Science*, 2018, **362**, 443-446.
3. W. Lai, Y. Jiao, Y. Liu, W. Fang, Z. Wang, M. D. Guiver and J. Jin, Engineering Ultra-Small Ag Nanoparticles with Enhanced Activity in Microporous Polymer Membranes for C₂H₄/C₂H₆ Separation, *Adv. Mater.*, 2025, **37**, 2416851.
4. S. Zhou, Z. Liu, P. Zhang, H. Rong, T. Ma, F. Cui, D. Liu, X. Zou and G. Zhu, Tailoring the pore chemistry in porous aromatic frameworks for selective separation of acetylene from ethylene, *Chem. Sci.*, 2022, **13**, 11126-11131.
5. X.-J. Xie, Y. Wang, Q.-Y. Cao, R. Krishna, H. Zeng, W. Lu and D. Li, Surface engineering on a microporous metal–organic framework to boost ethane/ethylene separation under humid conditions, *Chem. Sci.*, 2023, **14**, 11890-11895.
6. W. Liu, S. Geng, N. Li, S. Wang, S. Jia, F. Jin, T. Wang, K. A. Forrest, T. Pham,



- P. Cheng, Y. Chen, J. G. Ma and Z. Zhang, Highly Robust Microporous Metal-Organic Frameworks for Efficient Ethylene Purification under Dry and Humid Conditions, *Angew. Chem. Int. Ed.*, 2023, **62**, e202217662.
7. T. Lu, T. Xu, S. Zhu, J. Li, J. Wang, H. Jin, X. Wang, J. J. Lv, Z. J. Wang and S. Wang, Electrocatalytic CO₂ Reduction to Ethylene: From Advanced Catalyst Design to Industrial Applications, *Adv. Mater.*, 2023, **35**, 2310433.
 8. L.-L. Ma, P. N. Zolotarev, K. Zhou, X. Zhou, J. Liu, J. Miao, S. Li, G.-P. Yang, Y.-Y. Wang, D. M. Proserpio, J. Li and H. Wang, Three in one: engineering MOF channels via coordinated water arrays for regulated separation of alkanes and alkenes, *Chem. Sci.*, 2024, **15**, 19556-19563.
 9. J. Liu, H. Wang and J. Li, Pillar-layer Zn–triazolate–dicarboxylate frameworks with a customized pore structure for efficient ethylene purification from ethylene/ethane/acetylene ternary mixtures, *Chem. Sci.*, 2023, **14**, 5912-5917.
 10. D. S. Sholl and R. P. Lively, Seven chemical separations to change the world, *Nature*, 2016, **532**, 435-437.
 11. C. G. Morris, N. M. Jacques, H. G. W. Godfrey, T. Mitra, D. Fritsch, Z. Lu, C. A. Murray, J. Potter, T. M. Cobb, F. Yuan, C. C. Tang, S. Yang and M. Schröder, Stepwise observation and quantification and mixed matrix membrane separation of CO₂ within a hydroxy-decorated porous host, *Chem. Sci.*, 2017, **8**, 3239-3248.
 12. H. Wang, M. Shi, C. Wang, Z. Chu, Z. Yin and C. Wang, Superior Hydrogen Separation in Nanofluidic Membranes by Synergistic Effect of Pore Tailoring and Host–Guest Interaction, *Nano Lett.*, 2025, **25**, 9353–9361.
 13. T. Huang, Z. Su, K. Hou, J. Zeng, H. Zhou, L. Zhang and S. P. Nunes, Advanced stimuli-responsive membranes for smart separation, *Chem. Soc. Rev.*, 2023, **52**, 4173-4207.
 14. J. Qiao and D. Zhao, Ethane-gated MOFs meet industrial ethylene purification: Tiny gates open big possibilities, *Matter*, 2024, **7**, 2780-2783.
 15. X. Liu, G. Zhang, K. B. Al Mohawes and N. M. Khashab, Smart membranes for separation and sensing, *Chem. Sci.*, 2024, **15**, 18772-18788.
 16. X. Liu, Z. Wang, Y. Zhang, N. Yang, B. Gui, J. Sun and C. Wang, Gas-Triggered Gate-Opening in a Flexible Three-Dimensional Covalent Organic Framework, *J. Am. Chem. Soc.*, 2024, **146**, 11411-11417.
 17. Y. Ying, Z. Zhang, S. B. Peh, A. Karmakar, Y. Cheng, J. Zhang, L. Xi, C. Boothroyd, Y. M. Lam, C. Zhong and D. Zhao, Pressure-Responsive Two-Dimensional Metal–Organic Framework Composite Membranes for CO₂ Separation, *Angew. Chem. Int. Ed.*, 2021, **60**, 11318-11325.
 18. S. Feng, Y. Shang, Z. Wang, Z. Kang, R. Wang, J. Jiang, L. Fan, W. Fan, Z. Liu, G. Kong, Y. Feng, S. Hu, H. Guo and D. Sun, Fabrication of a Hydrogen-Bonded Organic Framework Membrane through Solution Processing for Pressure-Regulated Gas Separation, *Angew. Chem. Int. Ed.*, 2020, **59**, 3840-3845.
 19. C. Kang, Z. Zhang, S. Kusaka, K. Negita, A. K. Usadi, D. C. Calabro, L. S. Baugh, Y. Wang, X. Zou, Z. Huang, R. Matsuda and D. Zhao, Covalent organic



- framework atropisomers with multiple gas-triggered structural flexibilities, *Nat. Mater.*, 2023, **22**, 636-643.
20. K. T. Tan, S. Ghosh, Z. Wang, F. Wen, D. Rodríguez-San-Miguel, J. Feng, N. Huang, W. Wang, F. Zamora, X. Feng, A. Thomas and D. Jiang, Covalent organic frameworks, *Nat. Rev. Methods Prim.*, 2023, **3**, 1.
 21. W. Luo, H. Li, M. Jin, J. Liu, X. Zhang, G. Huang, T. Zhou and X. Lu, Organic frameworks (MOFs, COFs, and HOFs) based membrane materials for CO₂ gas-selective separation: A systematic review, *Sep. Purif. Technol.*, 2025, **357**, 130195.
 22. L. Li, H. Ma, J. Zhang, E. Zhao, J. Hao, H. Huang, H. Li, P. Li, X. Gu and B. Z. Tang, Emission-Tunable Soft Porous Organic Crystal Based on Squaraine for Single-Crystal Analysis of Guest-Induced Gate-Opening Transformation, *J. Am. Chem. Soc.*, 2021, **143**, 3856-3864.
 23. B. Yu, R.-B. Lin, G. Xu, Z.-H. Fu, H. Wu, W. Zhou, S. Lu, Q.-W. Li, Y. Jin, J.-H. Li, Z. Zhang, H. Wang, Z. Yan, X. Liu, K. Wang, B. Chen and J. Jiang, Linkage conversions in single-crystalline covalent organic frameworks, *Nat. Chem.*, 2023, **16**, 114-121.
 24. A. Yao, H. Xu, K. Shao, C. Sun, C. Qin, X. Wang and Z. Su, Guest-induced structural transformation of single-crystal 3D covalent organic framework at room and high temperatures, *Nat. Commun.*, 2025, **16**, 1385.
 25. F. Auras, L. Ascherl, V. Bon, S. M. Vornholt, S. Krause, M. Döblinger, D. Bessinger, S. Reuter, K. W. Chapman, S. Kaskel, R. H. Friend and T. Bein, Dynamic two-dimensional covalent organic frameworks, *Nat. Chem.*, 2024, **16**, 1373-1380.
 26. Z. B. Zhou, H. H. Sun, Q. Y. Qi and X. Zhao, Gradually Tuning the Flexibility of Two-Dimensional Covalent Organic Frameworks via Stepwise Structural Transformation and Their Flexibility-Dependent Properties, *Angew. Chem. Int. Ed.*, 2023, **62**, e202305131.
 27. L. J. Wayment, S. Huang, H. Chen, Z. Lei, A. Ley, S. H. Lee and W. Zhang, Ionic Covalent Organic Frameworks Consisting of Tetraborate Nodes and Flexible Linkers, *Angew. Chem. Int. Ed.*, 2024, **63**, e202410816.
 28. M. Wang, T. Zeng, Y. Yu, X. Wang, Y. Zhao, H. Xi and Y.-B. Zhang, Flexibility On-Demand: Multivariate 3D Covalent Organic Frameworks, *J. Am. Chem. Soc.*, 2023, **146**, 1035-1041.
 29. L. Zhang, B. Yu, M. Wang, Y. Chen, Y. Wang, L. B. Sun, Y. B. Zhang, Z. Zhang, J. Li and L. Li, Ethane Triggered Gate-Opening in a Flexible-Robust Metal-Organic Framework for Ultra-High Purity Ethylene Purification, *Angew. Chem. Int. Ed.*, 2024, **64**, e202418853.
 30. J. T. Damron, J. Ma, R. Kurz, K. Saalwächter, A. J. Matzger and A. Ramamoorthy, The Influence of Chemical Modification on Linker Rotational Dynamics in Metal–Organic Frameworks, *Angew. Chem. Int. Ed.*, 2018, **57**, 8678-8681.
 31. Y. Yang, L. Li, R.-B. Lin, Y. Ye, Z. Yao, L. Yang, F. Xiang, S. Chen, Z. Zhang, S. Xiang and B. Chen, Ethylene/ethane separation in a stable hydrogen-bonded



- organic framework through a gating mechanism, *Nat. Chem.*, 2021, **13**, 933-939. DOI: 10.1039/D0SC04964D
32. S.-M. Wang, M. Shivanna, S.-T. Zheng, T. Pham, K. A. Forrest, Q.-Y. Yang, Q. Guan, B. Space, S. Kitagawa and M. J. Zaworotko, Ethane/Ethylene Separations in Flexible Diamondoid Coordination Networks via an Ethane-Induced Gate-Opening Mechanism, *J. Am. Chem. Soc.*, 2024, **146**, 4153-4161.
 33. J. Liu, J. Peng, G. Chen, F. Lai, L. Dong, H. Ji and K. Chai, Hydroxyl-functionalized linker endows an ultra-microporous aluminum based metal-organic framework with electronegative site for enhancing ethane/ethylene separation, *Sep. Purif. Technol.*, 2024, **351**, 128116.
 34. G. D. Wang, Y. Z. Li, W. J. Shi, L. Hou, Y. Y. Wang and Z. Zhu, Active Sites Decorated Nonpolar Pore-Based MOF for One-step Acquisition of C₂H₄ and Recovery of C₃H₆, *Angew. Chem. Int. Ed.*, 2023, **62**, e202311654.
 35. H. M. Wen, C. Yu, M. Liu, C. Lin, B. Zhao, H. Wu, W. Zhou, B. Chen and J. Hu, Construction of Negative Electrostatic Pore Environments in a Scalable, Stable and Low-Cost Metal-organic Framework for One-Step Ethylene Purification from Ternary Mixtures, *Angew. Chem. Int. Ed.*, 2023, **62**, e202309108.
 36. N. Cao, H. Wang, Y. Ban, Y. Wang, K. Yang, Y. Zhou, M. Zhao, W. Deng and W. Yang, Tuning of Delicate Host-Guest Interactions in Hydrated MIL-53 and Functional Variants for Furfural Capture from Aqueous Solution, *Angew. Chem. Int. Ed.*, 2020, **60**, 1629-1634.
 37. Y. Li, J. Sui, L.-S. Cui and H.-L. Jiang, Hydrogen Bonding Regulated Flexibility and Disorder in Hydrazone-Linked Covalent Organic Frameworks, *J. Am. Chem. Soc.*, 2023, **145**, 1359-1366.
 38. B. Liu, X. Chen, N. Huang, S. Liu, Y. Wang, X. Lan, F. Wei and T. Wang, Imaging the dynamic influence of functional groups on metal-organic frameworks, *Nat. Commun.*, 2023, **14**, 4835.
 39. M. Chen, K. Yang, J. Wang, H. Sun, X. H. Xia and C. Wang, In Situ Growth of Imine-Bridged Anion-Selective COF/AAO Membrane for Ion Current Rectification and Nanofluidic Osmotic Energy Conversion, *Adv. Funct. Mater.*, 2023, **33**, 2302427.
 40. H. Wang, Y. Zhang, J. Wang, Sajilahu, H. Sun, H. Yang, X. H. Xia and C. Wang, In Situ Synthesized HOF Ion Rectification Membrane with Ultrahigh Permselectivity for Nanofluidic Osmotic Energy Harvesting, *Adv. Funct. Mater.*, 2024, **35**, 2412477.
 41. C. Wang, F. F. Liu, Z. Tan, Y. M. Chen, W. C. Hu and X. H. Xia, Fabrication of Bio-Inspired 2D MOFs/PAA Hybrid Membrane for Asymmetric Ion Transport, *Adv. Funct. Mater.*, 2019, **30**, 1908804.
 42. T. Wu, Y. Qian, Z. Zhu, W. Yu, L. Zhang, J. Liu, X. Shen, X. Zhou, T. Qian and C. Yan, Imine-Linked 3D Covalent Organic Framework Membrane Featuring Highly Charged Sub-1 nm Channels for Exceptional Lithium-Ion Sieving, *Adv. Mater.*, 2025, **37**, 2415509.
 43. M.-Y. Zhou, X.-W. Zhang, H. Yi, Z.-S. Wang, D.-D. Zhou, R.-B. Lin, J.-P. Zhang and X.-M. Chen, Molecular-Sieving Separation of Methanol/Benzene



Azeotrope by a Flexible Metal–Organic Framework, *J. Am. Chem. Soc.*, 2024, **146**, 12969-12975. [View Article Online](#)
DOI: 10.1039/D5SC04964D

44. V. I. Nikolayenko, D. C. Castell, D. Sensharma, M. Shivanna, L. Loots, K. A. Forrest, C. J. Solanilla-Salinas, K.-i. Otake, S. Kitagawa, L. J. Barbour, B. Space and M. J. Zaworotko, Reversible transformations between the non-porous phases of a flexible coordination network enabled by transient porosity, *Nat. Chem.*, 2023, **15**, 542-549.
45. X. Jing, M. Zhang, Z. Mu, P. Shao, Y. Zhu, J. Li, B. Wang and X. Feng, Gradient Channel Segmentation in Covalent Organic Framework Membranes with Highly Oriented Nanochannels, *J. Am. Chem. Soc.*, 2023, **145**, 21077-21085.
46. S. K. Sobczak, J. Drwęska, W. Gromelska, K. Roztocki and A. M. Janiak, Multivariate Flexible Metal–Organic Frameworks and Covalent Organic Frameworks, *Small*, 2024, **20**, 2402486.
47. X.-W. Zhang, D.-D. Zhou and J.-P. Zhang, Tuning the gating energy barrier of metal-organic framework for molecular sieving, *Chem*, 2021, **7**, 1006-1019.
48. K.-G. Liu, F. Bigdeli, A. Panjehpour, S. Hwa Jhung, H. A. J. Al Lawati and A. Morsali, Potential applications of MOF composites as selective membranes for separation of gases, *Coord. Chem. Rev.*, 2023, **496**, 215413.
49. D. Ao, Z. Yang, Z. Qiao, Y. Sun, Z. Zhang, M. D. Guiver and C. Zhong, Metal–Organic Framework Crystal–Glass Composite Membranes with Preferential Permeation of Ethane, *Angew. Chem. Int. Ed.*, 2023, **62**, e202304535.



Data Availability Statement

View Article Online
DOI: 10.1039/D5SC04964D

The data supporting the findings can be found in the article and ESI,[†] and are available from the authors upon reasonable request.

